arXiv:1410.2948v1 [cond-mat.supr-con] 11 Oct 2014

On the superconductivity of the Li_xRhB_y compositions

H. Takeya,[1] M. ElMassalami,[2] H. S. Amorim,[2] H. Fujii,[1] T. Mochiku,[1] and Y. Takano[1]

[1] *National Institute for Materials Science,1-2-1 Sengen, Tsukuba, Ibaraki 305-0047, Japan*
[2] *Instituto de Fisica, UFRJ, CxP l68528, 21945-970, Rio de Janeiro, Brazil*

We observed superconductivity ($T_c \simeq$2-3 K) in Li_xRhB_y intermetallics wherein x and y vary over a wide compositional range. The crystal structure consists of cubic unit-cell ($a \simeq 12.1$ Å) with centrosymmetric space group $Pn\bar{3}n$. A weak but positive pressure-induced increase of T_c was observed. The correlations between the composition and each of the followings were followed over a wide range of x and y: the unit-cell dimensions, T_c, Sommerfeld coefficient γ, Debye temperature θ_D, and critical fields H_{c1} and H_{c2}. The thermal evolution of the electronic specific heat within the superconducting phase was observed to follow a quadratic-in-T behavior. In addition, a paramagnetic Meissner Effect (PME) is manifested during a low-field-cooled magnetization cycle. This manifestation of quadratic-in-T behavior and PME feature will be discussed.

I. INTRODUCTION

Recently we reported[1] the observation of superconductivity ($T_c \approx 2$ to 3 K at ambient pressure) in a novel ternary Li_xRhB_y phase. This phase was found to be stable over a wide range of the Li and B content (namely $0.6 < x < 2, 1 < y < 2$) while maintaining (i) the same cubic unit-cell (∼12.1 Å, see Fig. 1), (ii) the same normal-state properties (e.g. Sommerfeld constant γ ∼3 mJ/molK^2 and Debye temperatures θ_D ∼250K), and (iii) the same superconducting properties (e.g. T_c ∼3K, $H_{c1}(0)$ ∼65Oe, $H_{c2}(0)$ ∼14 kOe). It happened that there is a difficulty in reconciling its thermodynamic properties with the reported symmetry of its crystal structure (see below).[1] In this work we resolve this difficulty by carrying out extensive structural, magnetic, magnetoresistivity, and thermal characterizations.

Our earlier structural analysis showed that based on the observed extinction rule [absence of $(00l)$ lines for l=odd], the possible space groups was proposed to be either $P2_13$ or $P4_232$. Given that these groups are characterized by a non-centrosymetric feature and that the Rh atom has a high Z-number, then it was concluded that Anisotropic Spin-Orbit Coupling, ASOC, effects should be manifested.[2–5] In general, the presence of such ASOC would lead to characteristic features such as: (i) A removal of the spin degeneracy which, in turn, would lead to an enhanced normal-state Pauli paramagnetism. (ii) An admixture of even-parity spin-singlet and odd-parity spin-triplet pairing states which may cause a manifestation of nodes in the structure of the quasiparticle gap function. As a results of such ASOC influences, many thermodynamical properties should exhibit a characteristic thermal evolution:[2–5] e.g. (i) the superconducting specific heat, $C_S(T < T_c)$, should manifest a power-in-T behavior,[2–5] (ii) the susceptibility of the superconducting state should be increased, and (iii) the upper critical field $H_{c2}(0)$ should exceed the Pauli paramagnetic limit $H_p \cong 3k_BT_c/\mu_B\sqrt{2}$.[6]

Our earlier thermodynamical characterization on Li_xRhB_y indicated that while $C_S(T < T_c)$ does exhibit a quadratic-in-T behavior (expected for line nodes), neither the susceptibility nor the evolution of $H_{c2}(T)$ curve confirm such an unconventional character. One of the objectives of the present work is to address this contradiction.

It is shown below that the present structural analysis, carried out on more than four dozens of samples, indicate that the space group of these Li_xRhB_y compositions is the *centro-symmetric* $Pn\bar{3}n$ rather than the earlier reported *non-centro-symmetric* $P2_13$ or $P4_232$:[1] this remove the contradiction between structural and thermodynamic properties. On the other hand, the above-mentioned contradiction among the thermodynamic properties will be discussed in term of conventional (rather than nonconventional) influences. Finally, we followed the evolution of the superconducting properties with the variation in the hydrostatic pressure as well as in the structural and material properties of these compositions (e.g. the unit-cell volume, stoichiometry, sample purity, defects concentrations ..etc.).

II. EXPERIMENTAL

To the best of our knowledge, the stabilization of ternary Li-Rh-B compound was reported only for the following nonsuperconducting cases: (i) the hexagonal Li_2RhB_2 (a =8.45 Å and c =4.287 Å),[7] and (ii) the orthorhombic $Li_2Rh_3B_2$ (a =5.7712 Å, b =9.4377 Å, c =2.8301 Å).[8] Badica *et al.*[9] attempted a synthesis of Li_2Rh_3B but the product was found to be multi-phasic consisting mainly of binary boride and elemental Li and B.

Polycrystalline samples of various Li_xRhB_y compositions ($0.4 \leq x \leq 3$ and $1 \leq y \leq 2$) were synthesized by standard solid state reaction of pure Li lump (99.9 %), Rh powder (99.95 %), and crystalline B powder (99 %). Rh and B were, first, mixed and pressed into pellets and afterwards, together with Li lump, were placed in a Ta foil or a BN crucible and sealed in a stainless container under an argon atmosphere. The container was heated up to 700-900 °C for 20 h and followed by furnace cooling. Afterwards these products were annealed

at the same temperature range.

The weight loss during the heating process was found to be less than 0.2 %. This result had been confirmed by the elemental analysis which was conducted using the Inductively Coupled Plasma (ICP) method on representative samples. Before the analysis, we used aqua regia first and then $K_2S_2O_7$ to completely dissolve Rh. The analytical determinations of each element (given in Table I) are close to the nominal compositions: an assuring result considering that both Li and B are light elements and the former is volatile.

Structural analysis of all investigated polycrystalline samples were carried out on a monochromatic Cu K_α diffractometer equipped with a Si detector (representative diagrams are shown in Fig. 1). Magnetization curves were measured on a superconducting quantum interference device (SQUID) magnetometer. Bulk samples were cut into a cylindrical shape (ϕ0.45 x0.50 cm) and sealed in a gelatin capsule (all handled in an inert-gas glove box). Pressure-dependent magnetization curves were measured with a low-temperature hydrostatic micro pressure cell (up to 1 GPa) operated within a SQUID environment. Daphne oil was used as a pressure-transmitting fluid while Sn as a manometer. Magnetoresistance curves were measured on parallelepiped samples of typical 0.11x0.12x0.45 cm^3 dimensions. We used a conventional DC, four-points method (1 mA) in a home-made probe which was operated within the environment of the above-mentioned magnetometer. Zero-field specific heat measurements were carried out on a semi-adiabatic calorimeter operating within the range of 0.5 $< T <$23 K with a precision better than 4%.

During all experiments, care was exercised so as to avoid air/moisture exposure since such exposure was found to cause a dimming of metallic luster and, furthermore, a reduction in both T_c and superconducting volume fraction. As such, samples were usually covered with apiezon N grease and guarded in an inert atmosphere (for remeasurement, grease was wiped off).

Some samples show double superconducting transitions in the magnetization, resistivity, or specific heat. Given that T_c of these transitions are $\sim$ 2 to 3 K and that the measured diffractograms do not exhibit any of the known superconducting contaminant phases (see caption of Fig. 1 and text below), then the manifestation of such double transitions is most probably related to the granular character of these samples or to an unknown ternary phase.

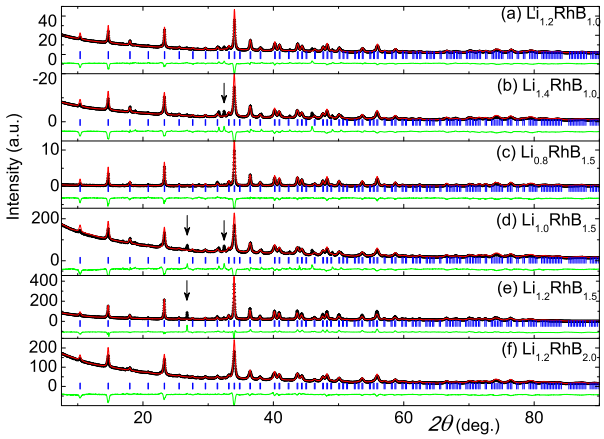

FIG. 1. (*Color Online*) Representative room-temperature X-ray diffractograms of Li_xRhB_y emphasizing the stability of the almost single-phase cubic structure in spite of the wide variation in x and y. *Symbols*: measured intensities; *short bars*: the Bragg positions, *lower thin line*: the difference curve; *solid line*: Rietveld calculated pattern using $Pn\bar{3}n$ (see text). The extremely weak impurity lines (the more intense, marked with short vertical arrow) are found to be related to nonsuperconducting $Li_2Rh_3B_2$ (more evident at $x >$ 1and $y \approx 1.5$), nonsuperconducting RhB (more evident at $x < 1$ and $y \approx 1$) and an unknown tetragonal phase (more evident at $0.4 < x < 1.5$ and $y \approx 1$).

III. RESULTS

A. Structural Analysis

Extensive structural and elemental analyses were carried out on more than four dozens of Li_xRhB_y compositions covering the range of $0.6 \leq x \leq 1.4$ and $0.5 \leq y \leq 2$ while keeping Rh stoichiometry fixed. As can be seen in the representatives Figs. 1-2(upper panel) and Table I as well as the electron diffraction patterns of Ref. 1, the almost single phase is stable over the range $0.8 \leq x \leq 1.5$ and $1 \leq y \leq 2$ but its concentration is strongly decreased when x or y is far from this range. All related Bragg lines can be indexed if one adopts a large-sized cubic unit-cell (see, e.g., Fig. 1).

The wide variation in Li and B content as well as their low atomic scattering factors make it extremely difficult to ascertain correctly their stoichiometry or to calculate the involved density. Nonetheless, application of extinction rules on resolution-improved diffractograms suggested that the space group is the centrosymmetric $Pn\bar{3}n$. Furthermore, using Le-Bail method and Patterson maps, the atomic position of the heavier Rh atoms are conclusively identified (for more details see Ref.10): Rh occupies the Wyckoff positions 48i and 12e. Furthermore, it seems that B occupies the position 8c leading to the formation of some distorted and others undistorted octahedrons: a features also common in other Rh-B compositions. It is noted that although these structural considerations lead only to partial determination and that further elucidation requires the identification of the exact stoichiometry and positions of Li and B atoms (a task which would be much effectively served by using, e.g., neutron diffraction analysis), nonetheless the calculated Rietveld patterns (Fig. 1) compares favorably with experiments and, as such, confirm the correct identification of the space group, all Rh positions, and one position of B.[10] Another encouraging evidence is that on

TABLE I. Some parameters of Li_xRhB_y compositions where x and y represent the measured content of Li and B relative to Rh as determined by ICP method; a is the parameter of the cubic cell (standard deviation reflects the variation associated with differing sample batches); the onset T_c as determined from magnetization, resistivity, or specific heat curves; $H_{c1}(0\ \mathrm{K})$ as determined from the magnetization curves; $H_{c2}(0\ \mathrm{K})$ as determined from the magnetoresistivity curves; β , γ, and δ_L coefficients as determined from the specific heat measurements. θ_D is estimated to be within the range 240 - 260 K. The coherence length $\xi(0)$ and the penetration depth $\lambda(0)$ were calculated from the following Ginzburg-Landau (GL) expressions: $H_{c2}(t) = \Phi_0/(2\pi\xi(0)^2(1\text{-}t))$ and $H_{c1}(0) = \Phi_0/[(4\pi\lambda(0)^2\ln(\lambda(0)/\xi(0))]$, where Φ_0 is the flux quantum and $t=T/T_c$. The calculated $H_{c2}(0\ \mathrm{K})$ was determined from the quadratic and WHH expressions (see text).

Nominal	measured		T_c	a	$H_{c1}(0)$	$H_{c2}^{quad}(0)$	$\xi(0)$	$\lambda(0)$	α	$H_{c2}^{WHH}(0)$	γ	β	δ_L
x,y	x	y	K	Å	Oe	kOe	nm	nm		kOe	mJ/molK^2	mJ/molK^4	J/molK
$Li_{0.8}RhB_{1.5}$	0.87	1.47	2.4	12.079(1)	83.5	13.7	15.5	15.7	0.29	9.6	3.3	0.46	0.024
$Li_{1.0}RhB_{1.5}$	0.95	1.48	2.6	12.086(7)	77	8.1	20.2	20.6	0.17	5.6	2.8	0.37	0.024
$Li_{1.2}RhB_{1.5}$	1.02	1.52	2.6	12.089(9)	65.6	14.2	14.4	14.5	0.3	9.8	2.4	0.40	0.024

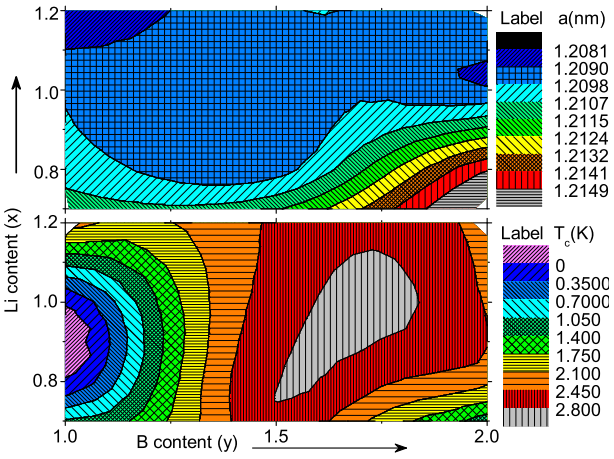

FIG. 2. (*Color online*) A partial section of two contour plots representing the evolution of the a-parameter (upper panel) and T_c (lower panel) of Li_xRhB_y with the Li (x) and B (y) content. These plots are constructed from compositions with fixed y=1, 1.25, 1.5, 1.75, 2 while varying x=0.4, 0.6, ..., 1.8, 2. It is cautioned that, our lowest measuring temperature is 1.8 K, accordingly all T_c below 1.8 K are generated by the interpolating plotting subroutine. The observed correlations are discussed in the text.

taking Li_xRhB_y with, say, $x, y \approx 1$ or 1.5, one calculates a density of 6.8 to 7.3 g/cm^3 which is comparable to 7.35 g/cm^3 of $Li_2Rh_3B_2$;[8] unfortunately, due to the strong porous character of these materials, we were unable to measure their density by conventional methods.[10]

The correlation of the unit-cell a-parameter with the Li/B content is shown in the upper contour plot of Fig. 2: evidently, on fixing Li (B) content and varying B (Li) concentration, the evolution of the a-parameter does not reflect any Vegard's law. In fact, a variation in the small-sized Li and B in Li_xRhB_y over the whole range of $0.4 \leq x \leq 3$ and $1 \leq y \leq 2$ modifies the unit-cell volume by only 1.1%: this emphasizes the crucial role of Rh sublattice.

B. Magnetization

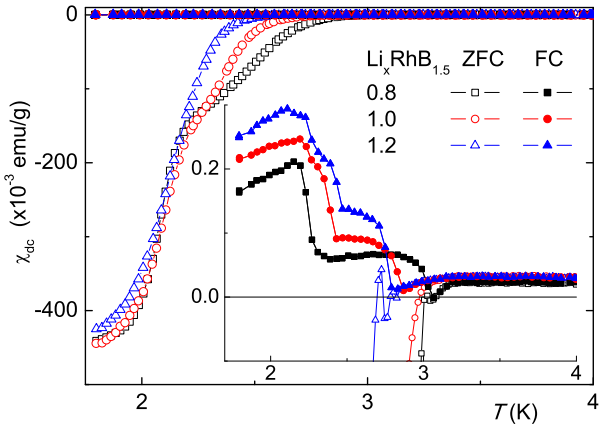

FIG. 3. (*Color online*) DC susceptibility curves of $Li_xRhB_{1.5}$ (x=0.8, 1.0, 1.2) at 20 Oe on ZFC (open symbols) and FC (filled symbols) cycles. *Inset*: an expanded view showing the typical character of the PME: on FC, just below T_c, $\chi(T)$ becomes negative and afterwards, on further cooling, turns into a positive value. By contrast, the ZFC susceptibility exhibits the normally-expected (negative) screening signal. The magnitude of the PME signal at $H = 20$ Oe is ~0.1% of the shielding ZFC signal (this is reminiscent of the PME in Nb disk[11]). The structure in both ZFC and FC curves within the immediate neighborhood below T_c is related to the fact that, within this region, the critical currents associated with most of the PME loops are too small to drive spontaneous moments.[12–14]

Zero-Field-Cooled (ZFC) magnetization of Li_xRhB_y (Fig. 3) exhibit a strong shielding signal. Field-Cooled (FC) magnetization, on the other hand, indicates a Paramagnetic Meissner Effect (PME): a negative drop immediately below T_c followed by a surge of a net (positive) paramagnetism, indicative of spontaneous magnetic moment, well below T_c. The XRD diffractograms of these three representative samples are shown in Fig. 1(c, d, e), each is practically a single-phase cubic structure. This together with the observed thermal evolution of this effect

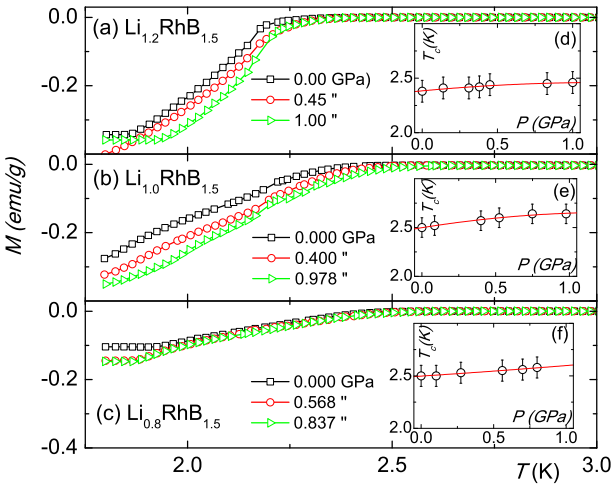

FIG. 4. (*Color online*) Pressure-dependent magnetization curves of (a) $Li_{1.2}RhB_{1.5}$, (b) $LiRhB_{1.5}$, and (c) $Li_{0.8}RhB_{1.5}$. *Insets*: the evolution of T_c with the applied pressure is approximated as (p in GPa): (d) $T_c \approx 2.38+0.13p-0.05p^2$ K for $Li_{1.2}RhB_{1.5}$, (e) $T_c \approx 2.50+0.24-0.09p^2$ K for $Li_{1.0}RhB_{1.5}$ and (f) $T_c \approx 2.50+0.09+0.01p^2$ K for $Li_{0.8}RhB_{1.5}$.

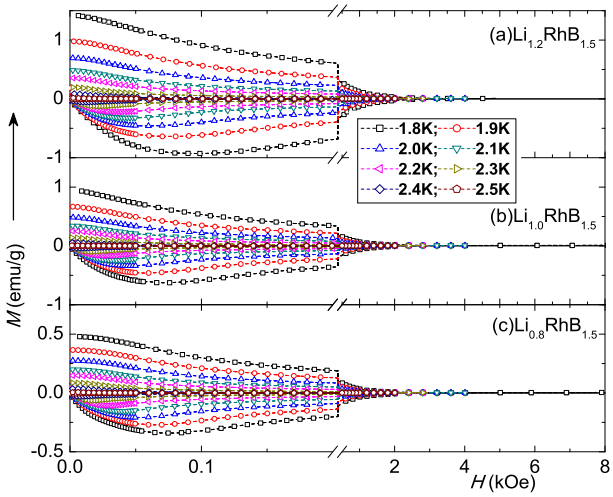

FIG. 5. (*Color Online*) Isotherm $M(H)$ curves of $Li_xRhB_{1.5}$: (a) x=1.2, (b) x=1.0, (c) x=0.8. For clarity, the ordinate scale of the lower panel was expanded by a factor of two.

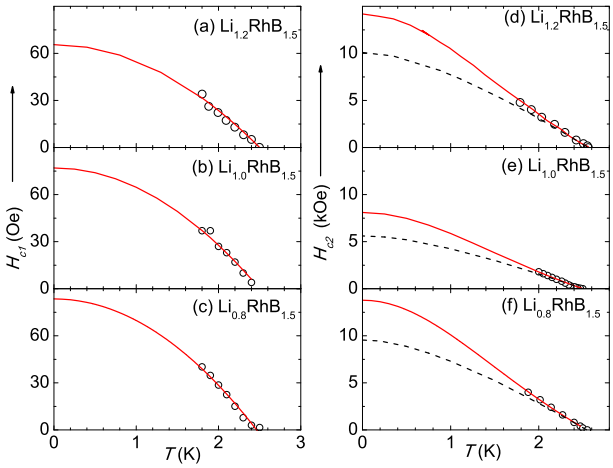

FIG. 6. (*Color Online*) (a, b, c): Measured $H_{c1}(T)$ (symbols) of $Li_xRhB_{1.5}$ were fitted (solid lines) to the relation $H_{c1} = H_{c1}(0)(1-t^2)$, where $t = T/T_c$. (d, e, f): measured $H_{c2}(T)$ of $Li_xRhB_{1.5}$ (symbol) were analyzed using (i) the quadratic formula $H_{c2}(t) = H_{c2}[(1\text{-}t^2)/(1+t^2)]$ (solid line) and (ii) the WHH expression (dashed lines).

(as well as that of isothermal field-dependent magnetization for $H > H_{c2}$) indicate that it is not related to an extrinsic contaminating paramagnetic centres. Generally, PME appears in granular superconductors wherein inverse Josephson Couplings (the so-called π contacts) are formed at the boundaries of multiply-connected superconducting grains.[12–14] Such boundaries may arise either due to extrinsic (such as disorder or impurity) or intrinsic factors (such as boundaries that connect differently oriented crystallites of superconductors with unconventional pairing[14]). As that the space group is centrosymmetric then no strong ASOC effects are expected and the presence of PME is most probably related to extrinsic factors or extreme porosity:[10] indeed the strength of the PME varies within different batches of the same sample.

The obtained T_c is shown as a function of the Li/B content in Fig. 2: T_c reaches a maximum within an approximate triangle-shape region having (x, y) vertices as (0.8, 1.5), (1.0, 1.8) and (1.2, 1.6). Accordingly, the three $Li_xRhB_{1.5}$ ($x = 0.8, 1.0, 1.2$) samples were extensively studied since they are faithful representatives of the whole series. Their a-parameters stabilize around 12.08-12.10 Å (see Fig. 2). Furthermore, a variation in their Li/B content influences T_c, most probably through an induced variation in $N(E_F)$, Debye temperature θ_D, or pairing interaction U [e.g. as in the BCS relation $T_c = 0.85\theta_D \exp(-1/UN(E_F))$]. As most of these parameters can be varied through pressure, we investigated as well the influence of applied pressure (p) on the superconductivity of these Li_xRhB_y compositions. The pressure-dependent magnetization (Fig. 4) indicates that both the superconducting fraction and T_c are weakly enhanced. In particular, for pressure up to 1 GPa and to a second order in p, $T_c \approx T_{c0} + d_1p + d_2p^2$ (p in GPa) where T_{c0}= 2.50, 2.50, 2.38 K; $d_1 = \frac{\partial T_c}{\partial p}$=0.09, 0.24, 0.13 K/GPa; $d_2 = \frac{\partial^2 T_c}{2\partial p^2}$= 0.01,-0.09, -0.05 for $Li_xRhB_{1.5}$ (x=0.8,1.0,1.2, resp.). Evidently the overall pressure influence is almost linear and rather weak. Relatively, $Li_{1.0}RhB_{1.5}$ (mid-panel of Fig. 4) exhibits a more pronounced P-induced variation.

Figure 5 shows the isothermal magnetization curves of $Li_xRhB_{1.5}$: typical type-II curves with no strong positive normal-state paramagnetic susceptibility (absence of strong polarization). This latter result is in agreement with the same features exhibited in Figs. 3-4: all confirm the absence of ASOC effects. Based on these isothermal curves of Fig. 5, we determined the thermal

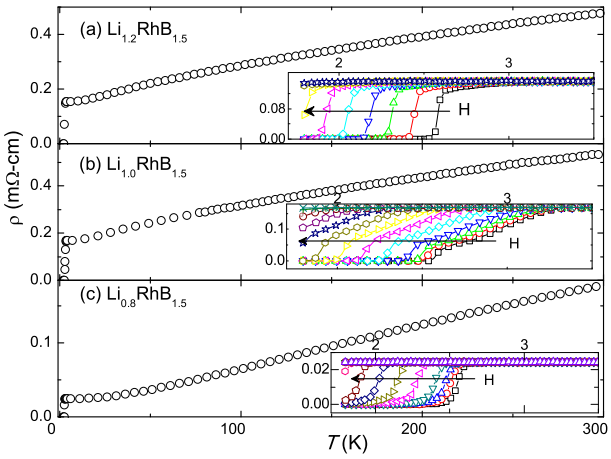

FIG. 7. Zero-field resistivity versus temperature of (a) $Li_{1.2}RhB_{1.5}$, (b) $Li_1RhB_{1.5}$, and (c) $Li_{0.8}RhB_{1.5}$ samples showing a normal-state metallic character above T_c. Insets: the magnetoresstivity across the superconducting transition region. For clarity, the ordinate scale of the lower panel was expanded by a factor of two.

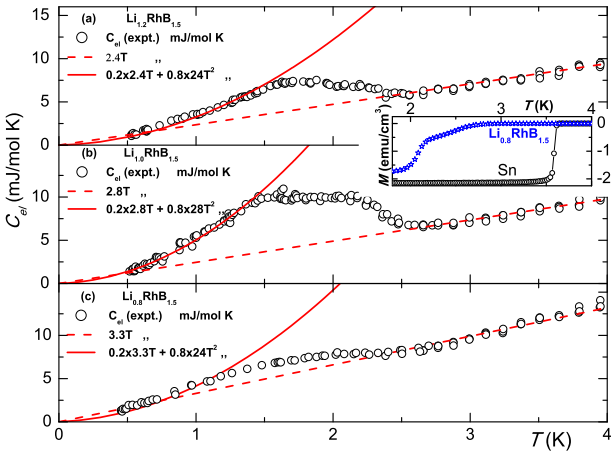

FIG. 8. (*Color Online*) The electronic specific heat contribution of (a) $Li_{1.2}RB_{1.5}$, (b) $Li_{1.0}RB_{1.5}$ and (c) $Li_{0.8}RB_{1.5}$ obtained after subtracting the calculated Debye contribution: $C_{el} = C_{tot} - \beta T^3$. The dashed lines are least-square fits to $C_{el} = \gamma T$ while the solid thick lines represent the calculation $0.2(\gamma T) + 0.80.\alpha_L\,(T/T_c)^2$ (see text). The specific heat jump at T_c is not sharp but the structure, just below T_c, is evident as in the magnetization curve (see inset). *Inset*: As a representative, the diamagnetism of $Li_{0.8}RB_{1.5}$ is 80% of that of a Sn sample having the same shape and size; this is attributed to a presence of normal-state regions (see text).

evolution of H_{c1} (for H_{c2}, see below) which, as can be seen in Figs. 6(a-c), follows reasonably well the relation H_{c1}=$H_{c1}(0)$[1-$(T/T_c)^2$] wherein $H_{c1}(0)$ and T_c are as given in Table I.

C. Magnetoresistivity

The thermal evolution of the resistivity of $Li_xRhB_{1.5}$, $\rho(T_c < T \leq 300$ K), shown in Fig. 7, indicates a metallic normal state. For most samples, $\rho(T$ =300 K) ≤ 0.48 mΩ-cm while the residual resistivity (in the immediate range above T_c) is ≤ 0.12 mΩ-cm: that RRR∼4 suggests additional scattering processes (e.g. a random atomic distribution, interstitial or substitutional defects related to Li/B nonstoichiometry). Fig. 7 indicate also a superconducting state with a transition which, due to percolation, are much sharper and narrower than the ones observed in the magnetizations or specific heats. Because of these advantageous features, $H_{c2}(T)$, Fig. 6, was determined from the midpoint of the transition occurring in each of $\rho(T, H)$ curve of Fig. 7 rather than from the event occurring in each $M(H)$ isotherm of Fig. 5.

D. Specific Heat

The specific heats of Li_xRhB_y samples evolves, within $T_c < T < 5$ K, as $\gamma T + \beta T^3$ [Ref.1]: γ and β are given in Table I. Just like T_c and lattice parameter, there is a weak Li-dependence of both γ and β; γ, in particular, decreases slightly as Li content is increased.

The electronic contribution, $C_{el}(T)$, obtained after subtracting the Debye part (βT^3), is shown in Fig. 8. For a conventional BCS-type gapped superconductor, the electronic contribution below T_c is dominated by an exponential-in-T behavior. Fig. 8 does not show any exponential evolution and as such the gap is either not fully-developed or blurred by some anomalous behavior. The origin behind such a behavior may be revealed if one obtains an analytical expression of the thermal evolution of $C_{el}(T < T_c)$. But first let us evaluate whether C_{el} is due solely to the superconducting phase contribution. In that regard, the inset of Fig. 8 indicate that the typical superconducting shielding fraction of these samples is 80% of the signal obtained from a similar-sized Sn sample.[1] It was assumed that the residual normal-state gives rise to a $0.2\gamma T$ contribution. Fig. 8 indicates that the relation $C_{el}\,(T < T_c) = 0.2\gamma T + 0.8\delta_L\,(T/T_c)^2$ describes reasonably well the electronic contribution. The obtained values of δ_L are similar for all compositions, namely 24 mJ/molK: this suggests a correlation between δ_L and the electronic contribution of the Rh sublattice since such a contribution does not vary across the studied samples. Though the arguments given in Ref. 1 attributed such a quadratic-in-T behavior to line nodes, our present understanding (based on the above-mentioned crystallographic and thermodynamics arguments) is that this power relation may be related to distribution effects arising from, say, variation in the Li/B content (for evidences regarding $H_{c2}(0)$ see below).

IV. DISCUSSION AND CONCLUSIONS

Based on the correlation between T_c and the volume ($V = a^3$) shown in Fig. 2, one expects:

$$\frac{\partial T_c}{\partial p} = \frac{1}{V}\frac{\partial V}{\partial p}\frac{V\partial T_c}{\partial V} = \beta.V.\frac{\partial T_c}{\partial V},$$

where β is the compressibility of the solid. Although there are no information on $\beta(T,p)$, $V(T,p)$, or lattice anisotropy, it is possible to correlate the observed weak pressure-dependence of T_c with the general features of the upper panel of Fig. 2: these particular samples are situated within a Li/B region wherein the overall variation of T_c with V (thus with pressure) is weak; even more weaker dependence is observed for regions with an excess or deficiency of the Li content. From these features (see also Table I), it can be concluded that a variation in pressure or Li content (B is fixed) would not bring about any strong variation in T_c, $N(E_F)$, θ_D, or U.

The thermal evolution of each $H_{c2}(T)$ curve, shown in Figs. 6 (d-f), was analyzed in terms of (i) the quadratic Ginzburg-Landau relation $H_{c2}(t) = H_{c2}[(1-t^2)/(1+t^2)]$ and (ii) the Werthamer–Helfand–Hohenberg (WHH) expression[15,16] which is usually parameterized in terms of α (a measure of the Pauli spin effect) and λ_{so} (a measure of the spin-orbit scattering). While λ_{so} is a fit parameter, α is taken to be determined experimentally, based on the relation[15,16] $\alpha = 5.33 \times 10^{-5}(\partial H_{c2}/\partial T)_{T_c}$, giving 0.17, 0.29, 0.3 for x=0.8, 1.0 and 1.2, respectively. As expected, both descriptions of $H_{c2}(T)$ reproduce satisfactorily the measured curves within the range $T \to T_c$. In fact, both descriptions are reasonable within the available temperature range since this range is still very close to T_c ($t = T/T_c \to 1$). In general, the WHH description is more appropriate for the range $T \to 0$: accordingly, we used the relation $H_{c2}(0) = -0.693T_c(\partial H_{c2}/\partial T)_{T_c}$ to evaluate $H_{c2}(0)$ giving 5.6, 9.6 and 9.8 kOe for x=0.8, 1.0 and 1.2, respectively. Such $H_{c2}(0)$ values are surprisingly low. In fact it is one order of magnitude lower than the paramagnetic limit $H_p \cong 3k_BT_c/\mu_B\sqrt{2} \simeq 80$ kOe. As such this constitutes an additional evidence which (together with the above-mentioned ones) confirms the absence of ASOC effects. Indeed, in spite of the higher Z value of Rh, the WHH analysis of $H_{c2}(T)$ (Fig. 6) indicate no significant role for the λ_{so} parameter. Accordingly, $H_{c2}(T)$ in these Li_xRhB_y compositions is taken to be determined by the standard orbital driven depairing process.

In summary, Li_xRhB_y compositions form a new class of Li-based superconductors. The variation in Li/B ratio is accompanied by a weak change in the unit-cell length, in the normal-state properties (e.g. γ, β), and in the superconducting properties (e.g. $H_{c1}(0)$, $H_{c2}(0)$, and T_c). Many of the studied parameters are interrelated: as an example, the a-parameter and T_c are correlated and, furthermore, this same correlation is evident in the positive pressure dependence of T_c. As these materials are centrosymmetric superconductors, the observations of PME during the field-cooled $M(T)$ cycle and a quadratic-in-T superconducting specific heat are attributed to conventional (rather than nonconventional) features such as inhomogeneous distribution of defects or Li/B atoms. Indeed the thermal evolution of $H_{c2}(0)$ can be described by a conventional WHH expression. Finally, based on the observed correlation between composition, V and T_c of Li_xRhB_y, it would be very interesting to carry out a systematic study on the Li-M-X series (M= transition metal, X =B, As, Si, Ge).

ACKNOWLEDGMENTS

The authors are grateful to the "Foundation for Promotion of Material Science and Technology of Japan (MST Foundation)" for the financial support. We also acknowledge the partial support received from the Japan Society for the Promotion of Science.

[1] H. Takeya, H. Fujii, M. ElMassalami, F. Chaves, S. Ooi, T. Mochiku, Y. Takano, K. Hirata, and K. Togano, J. Phys. Soc. Jpn. **80**, 013702 (2011).

[2] M. Sigrist and K. Ueda, Rev. Mod. Phys. **63**, 239 (1991).

[3] E. Bauer, I. Bonalde, and M. Sigrist, Low Temp. Phys. **31**, 748 (2005).

[4] M. Sigrist, D. F. Agterberg, P. A. Frigeri, N. Hayashi, R. P. Kaur, A. Koga, I. Milat, K. Wakabayashia, and Y. Yanase, J.M.M.M, **310**, 536 (2007).

[5] P. A. Frigeri, D. F. Agterberg, and M. Sigrist, New J. Phys **6**, 115 (2004).

[6] P. Frigeri, D. Agterberg, A. Koga, and M. Sigrist, Physica B: Condensed Matter **359-361**, 371 (2005), proceedings of the International Conference on Strongly Correlated Electron Systems.

[7] W. Jung and B. Schmidt, Naturwissenschaften **63**, 583 (1976).

[8] M. S. Baileya, E. B. Lobkovskyb, D. G. Hinksa, H. Claus, Y. S. Hora, J. A. Schluetera, and J. F. Mitchella, J. Solid State Chem. **180**, 1333 (2007).

[9] P. Badica, K. Togano, H. Takeya, K. Hirata, S. Awaji, and K. Watanabe, Physica C **460-462**, 91 (2007).

[10] H. S. Amorim et al., To be published.

[11] D. J. Thompson, M. S. M. Minhaj, L. E. Wenger, and J. T. Chen, Phys. Rev. Lett. **75**, 529 (1995).

[12] D. Khomskii, Journal of Low Temperature Physics **95**, 205 (1994).

[13] M. S. Li, Physics Reports **376**, 133 (2003).

[14] M. Sigrist and T. M. Rice, Rev. Mod. Phys. **67**, 503 (1995).

[15] N. R. Werthamer, E. Helfand, and P. C. Hohenberg, Phys. Rev. **147**, 295 (1966).

[16] R. R. Hake, Phys. Rev. **158**, 356 (1967).